

# Pyrolysis and Oxidation of Waste Tire Oil: Analysis of Evolved Gases

Abdul Gani Abdul Jameel,\* Awad B.S. Alquaity, KM Oajedul Islam, Amjad Ali Pasha, Sikandar Khan, Medhat A. Nemitallah, and Usama Ahmed\*



Cite This: *ACS Omega* 2022, 7, 21574–21582

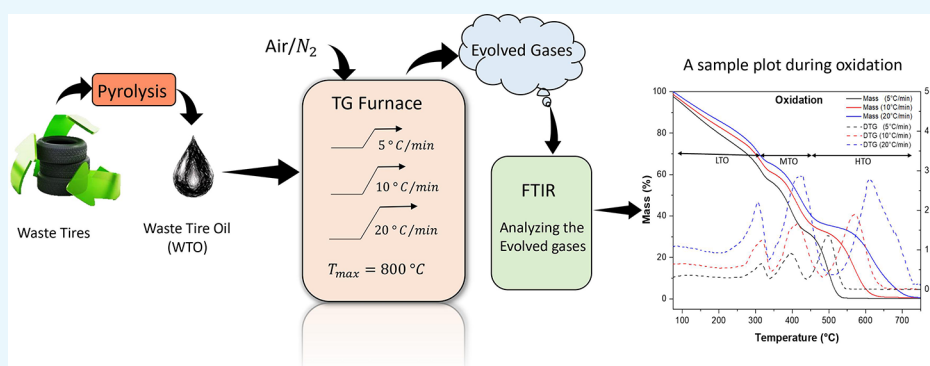


Read Online

ACCESS |

Metrics & More

Article Recommendations



**ABSTRACT:** Valorization of waste such as waste tires offers a way to manage and reduce urban waste while deriving economic benefits. The rubber portion of waste tires has high potential to produce pyrolysis fuels that can be used for energy production or further upgraded for use as blend fuel with diesel. In the present work, waste tire oil (WTO) was produced from the pyrolysis of waste tires in an electric heating furnace at 500–550 °C in the absence of oxygen. Pyrolysis (in nitrogen) and oxidation (in air) of the obtained WTO sample were then performed in a thermogravimetric (TG) furnace that was connected to a Fourier transform infrared cell where the evolved gases were analyzed. The WTO sample was heated up to 800 °C in the TG furnace where the temperature of the sample was ramped up at three heating rates, namely, 5, 10, and 20 °C/min. The TG mass loss and differential thermogravimetric mass loss plots were used to analyze the thermal degradation pathways. Kinetic analysis was performed using the distributed activation energy model to estimate the activation energies along the various stages of the reaction. The pollutant gases, namely, CO<sub>2</sub>, CO, NO, and H<sub>2</sub>O, formed during WTO oxidation were evaluated by means of the characteristic infrared absorbance. The functional groups evolved during pyrolysis, namely, alkanes, alkenes, aromatics, and carbonyl groups, were also analyzed. The obtained information can be used for the better design of gasifiers and combustors, to ensure the formation of high-value gaseous products while reducing the emissions. The utilization of waste tires by producing pyrolysis oils thus offers a way of tackling the menace of waste tires while acting as a potential energy source.

## 1. INTRODUCTION

Waste car tires are quickly becoming a menace of global proportions with more than 25.7 million tons of waste generated annually out of which 35% is not recycled or recovered in any shape or form.<sup>1</sup> Waste tires are typically aggregated and due to their low volume density and high void ratio, consume a relatively large space in landfills or dumping grounds. One of the several options to use waste tires is through producing pyrolysis oil, which is a liquid fraction obtained from their pyrolysis.<sup>2</sup> The use of waste tire oil (WTO) needs to be perceived in the broad context of the concept of circular economy, which is essential to move toward the new paradigm in sustainability.<sup>1</sup> The tires that are typically dumped in landfills can help meet some of the energy needs, which is evaluated as part of the current work. When looking at any recycling opportunity, it is imperative to understand the

net gain in energy obtained in reusing the resource as compared to dumping it in landfills or incinerators. The growing interest in transitioning from a linear economy to a circular economy coupled with the relatively large heating value of WTO (higher heating value between 40 and 44 MJ/kg) makes it particularly suitable for potential use as a fuel in numerous combustion systems<sup>3,4</sup> including as drop-in fuel blends in diesel engines.<sup>5</sup> Moreover, the presence of natural rubber in tires makes WTO even more attractive for

**Received:** March 7, 2022

**Accepted:** May 30, 2022

**Published:** June 14, 2022



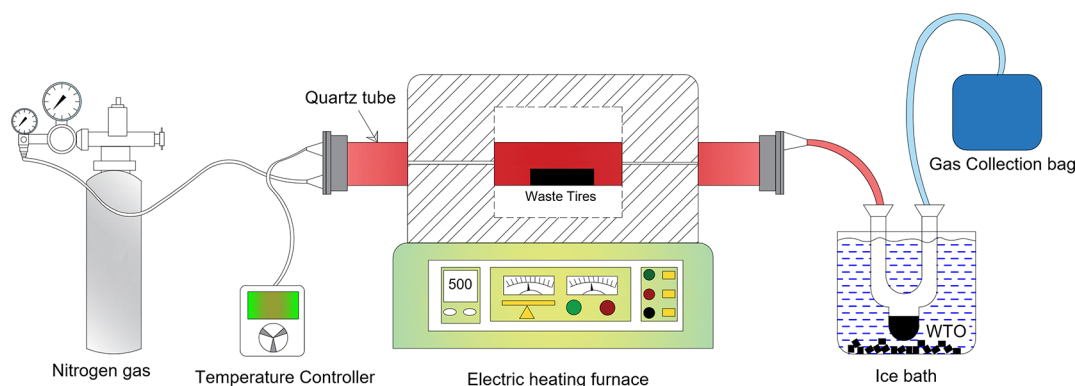


**Figure 1.** Schematic of the WT pyrolysis employed for WTO production.

combustion systems because of its near zero carbon or carbon recycling credentials.

The composition of WTO depends on the feedstock and the processes used for its conversion, which has been extracted using several characterization techniques including nuclear magnetic resonance (NMR),<sup>4,6</sup> thermogravimetric analysis,<sup>7–10</sup> and Fourier transform-ion cyclotron resonance (FT-ICR) mass spectroscopy.<sup>4</sup> However, these techniques are not designed to measure the composition of gases evolved during its pyrolysis or oxidation, which is essential for understanding the emissions during its combustion. Nevertheless, a thermogravimetric (TG) analyzer connected with a Fourier transform infrared (FTIR) cell can provide the required information on the composition of gases during combustion relevant processes. TGA-FTIR is an excellent technique capable of performing real-time, highly accurate, and robust measurements using a small sample size, which makes it an obvious candidate for characterizing a large number of fuels/chemicals including oil shale,<sup>11</sup> lignite blends,<sup>12</sup> biodiesel,<sup>13</sup> palm oil waste,<sup>14</sup> heavy fuel oil,<sup>15</sup> and biomass.<sup>14,16–19,46</sup>

TGA-FTIR analysis for waste tires has recently been performed in a number of studies to understand the pyrolysis mechanism and product distribution. Xu et al.<sup>20</sup> investigated the thermal decomposition and product distribution of a waste bicycle tire using TGA-FTIR and GC/MS techniques. They observed two distinct stages in the pyrolysis process representing rubber pyrolysis in the low-temperature stage (285–531 °C) and pyrolysis of the remaining products in the high-temperature stage (663–847 °C). The resulting FTIR spectra gathered at various temperatures pointed toward the release of aromatics in the high-temperature stage. Further pyrolysis measurements performed using a pyrolyzer coupled with GC-MS provided a detailed makeup of gaseous, alkenes, and aromatic components whose product distribution varied with temperature. The fast pyrolysis of waste tires was investigated by Menares et al.<sup>21</sup> using quasi-isothermal TGA and a pyrolyzer coupled with GC-MS. Moreover, kinetic modeling was performed to improve the understanding of the reaction pathways controlling waste tire pyrolysis. At temperatures less than 500 °C, limonene and isoprene were the major products, whereas formation of monoaromatics and gaseous products increased at temperatures above 600 °C. Li et al.<sup>22</sup> performed a similar detailed investigation into the pyrolysis of waste tires using TGA-FTIR/MS and a pyrolyzer coupled with GC-TOF/MS. A kinetic mechanism for waste tire pyrolysis was proposed using the dominant species observed in the pyrolysis measurements. The pyrolysis products were divided

into four main categories where aromatic species were dominant consisting mainly of methyl benzene, *para*-xylene, and mesitylene. The other important categories of products noticed were gases and aliphatic hydrocarbons.

The objective of the current investigation is to thoroughly evaluate the pyrolysis and oxidation of WTO using the TGA-FTIR technique. The mass loss characteristics in air (oxidation) and nitrogen (pyrolysis) are reported using TG and DTG plots. Furthermore, the emission of pollutant gases during oxidation and the evolution of functional groups during pyrolysis have also been studied by means of an FTIR cell that was coupled to a TG furnace. The evolved gases from WTO on account of heating were swept to an FTIR cuvette/cell. The absorbance bands of pollutant gases and functional groups present in the gases were analyzed to understand the nature of the gases evolved.

## 2. EXPERIMENTAL SECTION

**2.1. WTO Production.** Waste tire samples were collected from a recycling facility, and the rubber portion of the tire (without the netting and steel threads) was dried in a desiccator to remove any bound moisture content and then ground into powder. The size distribution of the tire particles was measured to be around 0.5–2 mm. The schematic of the WT pyrolysis process is presented in Figure 1. The waste tire particles were then placed in the center of a quartz tube that was placed inside an electric heating furnace. The quartz tube was then purged with nitrogen for 30 min at a flow rate of 0.5 L per minute to remove any oxygen present as air in the tube. The WT placed inside the quartz tube was then heated to a temperature of 500–550 °C by using an electric furnace, and a nitrogen carrier gas was supplied at a constant flow rate of 0.2 L per minute. The temperature was closely monitored by using a thermocouple, and heating was continued for a period of 1 h. The nitrogen gas containing the evolved gases from waste tire pyrolysis was then pumped through an ice bath, where the gases were condensed to yield WTO. The physical and chemical properties of the obtained WTO are presented in Table 1. The obtained WTO sample has a kinematic viscosity of  $2.88 \times 10^{-6}$  m<sup>2</sup>/s, which is in the range for diesel fuels. It also has an appreciable higher heating value (HHV) of 40.9 MJ/kg, which indicates its potential for energy applications.

**2.2. TGA-FTIR System.** Pyrolysis and oxidation of the WTO sample were performed in a Shimadzu TGA 51H analyzer that was coupled to an FTIR cell (Nicolet Magna IR-560). The samples were heated inside a TGA furnace from the initial room temperature of 25 °C to a final set furnace

**Table 1. Properties of WTO**

property	unit	value
density (at 15 °C)	kg/m <sup>3</sup>	908.1
kinematic viscosity (at 40 °C)	m <sup>2</sup> /s	2.88 × 10 <sup>-6</sup>
HHV	MJ/kg	40.9
ultimate analysis (mass %)		value
carbon		86.82
hydrogen		10.21
nitrogen		0.66
sulfur		0.40
oxygen		1.91

temperature of 800 °C at three heating rates, namely, 5, 10, and 20 °C/min. Blank tests were also performed with empty pans in the furnace to account for any buoyancy effects. The evolved gases in the furnace were carried to the FTIR cell by employing nitrogen as a carrier gas. The connection between the TG furnace and the FTIR cell was established using a heated line constantly maintained at 200 °C to prevent the gases from condensing. The FTIR spectra were recorded once every 10 s with a resolution factor of 4 cm<sup>-1</sup>. The spectra were collected at wavenumbers ranging from 4000 to 500 cm<sup>-1</sup>.

### 3. RESULTS AND DISCUSSION

**3.1. WTO Pyrolysis.** TG and DTG curves for the pyrolysis of WTO are shown in Figure 2 at the three heating rates as

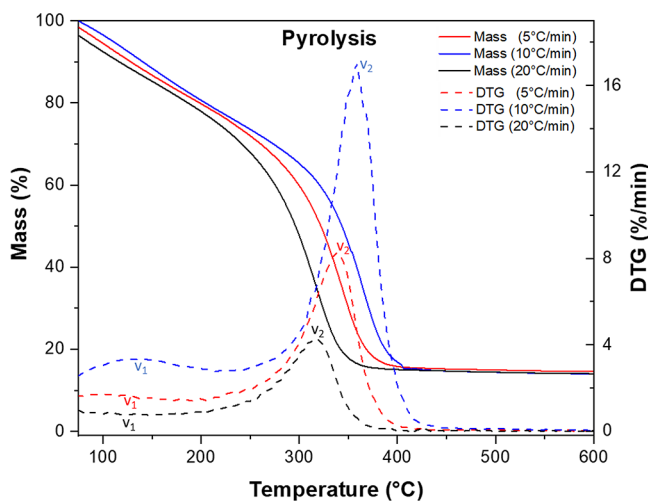


**Figure 2.** TG and DTG plots of the pyrolysis of WTO in a nitrogen atmosphere.

previously mentioned. The inert environment was maintained by supplying nitrogen gas. Under pyrolysis conditions, devolatilization, i.e., the release of volatile components, occurs due to thermal degradation of the WTO sample as the temperature of the sample is continuously ramped up. The first phase in the pyrolytic devolatilization of WTO is the evolution of low-boiling species like alkanes and alkenes present in WTO. It has also been shown that during devolatilization, the alkyl side chains of heavier aromatic structures are cleaved, which result in the release of low-boiling and light components like methane, ethane, ethylene, etc. The maximum mass loss during this first phase is denoted by  $v_1$  in the DTG curve and shown in Figure 2, and the corresponding temperatures noticed were 118, 125, and 134 °C for heating rates of 5, 10,

and 20 °C/min, respectively. Then, as the temperature increased, the rate of mass loss was observed to decrease. This happens because of the diminution of the light components in the fuel.

The rate of mass loss then increases sharply as the temperature is increased. It reaches to peak values at 322, 340, and 359 °C for heating rates of 5, 10, and 20 °C/min, respectively. This maximum mass loss is expressed by the notation  $v_2$ . This represents the second phase of the devolatilization where the emission of compounds with higher boiling points like aromatics likely occurs. The rate of mass release decreases with a further increase in the temperature due to the exhaustion of the volatile content. Finally, it reaches to a minimum value that indicates the termination of the second phase and of the devolatilization. The remaining part of the sample is the carbonaceous fraction (approximately 16% of the initial mass), which shows very little degradation on further heating.

**3.2. WTO Oxidation.** The oxidation of WTO in the presence of O<sub>2</sub> is relatively more complex compared to pyrolysis as it involves numerous simultaneous reactions due to the complex and multicomponent nature of WTO. Figure 3

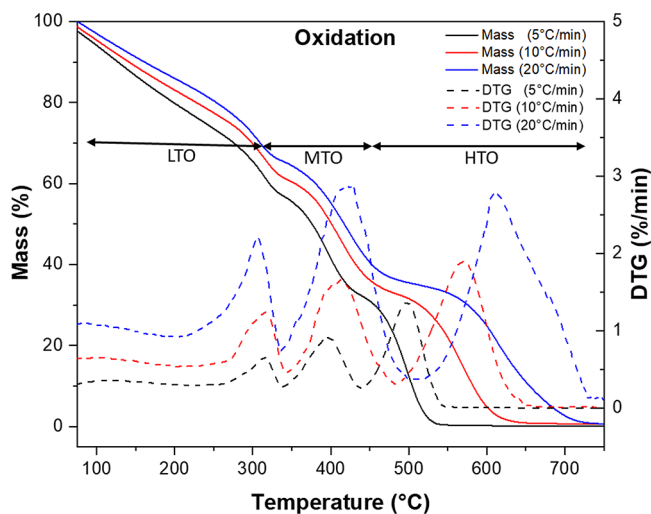


**Figure 3.** TG and DTG plots of the oxidation of WTO.

illustrates the oxidation of WTO for a wide range of temperatures at different heating rates. From the DTG plot, the oxidation of the fuel can be divided into three phases. During the initial phase termed as low-temperature oxidation (LTO), the sample undergoes devolatilization similar to the phases involved in pyrolysis. This stage extends up to 340, 344, and 336 °C for heating rates of 5, 10, and 20 °C/min, respectively. It reaches to peak points where the rate of mass loss is the highest noticed at 319, 324, and 315 °C for the mentioned heating rates. As the temperature was further increased, the rate of mass release was found to decrease, thus concluding the LTO.

In the next phase termed as mid-temperature oxidation (MTO), oxidation of the released gaseous components occurs. The high temperature and the presence of metals like Ni and V shown to be present in tire pyrolysis oils work as catalysts that also cause liquid phase oxidation of the fuel.<sup>23</sup> The rate of mass loss observed in the MTO phase was observed to be the highest as volatile fractions of the fuel continuously break and form skin-like structures.<sup>15,24,25</sup> This stage ends at 441, 484,

and 512 °C for the various heating rates discussed. At the end of this phase, only a carbonaceous form of the fuel remains with a high carbon to hydrogen (C/H) ratio possessing pores and cracks throughout its volume. This introduces a mass transfer resistance, and as a result, the rate of mass loss decreases.

The final phase of WTO oxidation is the high-temperature oxidation (HTO). It ranges from 441 to 540 °C, 484 to 651 °C, and 512 to 730 °C for the discussed heating rates. In this stage, the rate of mass loss reduces to less than 1%/min as it reaches the end. Char oxidation in the form of heterogeneous surface reactions occurs at this stage with an extensive mass loss.<sup>26</sup> Available pores and cracks allow the oxygen to diffuse through them easily, which results in the complete oxidation of the WTO sample. Around 0.4–0.5% of the initial weight of the sample is left at the end, which comprises mostly ash and unburnt char particles. The profile of the TG and DTG curves obtained during WTO oxidation showing the three stages has also been observed for a number of fuel oils<sup>24,27–29</sup> that closely resemble WTO.

**3.3. Kinetic Analysis.** As seen from the TG and DTG plots, pyrolysis and combustion of WTO are complex phenomena that proceed with various stages/reactions, and as a result, the activation energy changes with the conversion. Kinetic analysis was performed using the distributed activation energy (DAE) model<sup>30,31</sup> to determine the variation in the activation energy ( $E$ ) during WTO pyrolysis and oxidation. The chosen model can provide both the pre-exponential factor and activation energy using which the TG mass loss profile can be generated. The DAE model was chosen as it has been applied to a number of samples compositionally similar to WTO.<sup>15</sup> A first-order reaction is assumed by the DAE model, which is given by the following equation:

$$\frac{d\alpha}{dT} = \frac{A}{\beta} e^{-E/RT} (1 - \alpha) \quad (1)$$

where  $\alpha$  stands for conversion,  $T$  for temperature,  $A$  for the pre-exponential factor, and  $\beta$  for the TG heating rate employed. Applying a logarithm to eq 1 results in the equation of a straight line of the form  $y = mx + c$ . Plotting  $\ln(\beta d\alpha/dT)$  in the Y axis and  $1/RT$  at a given conversion value helps to calculate the activation energy for various conversion heating rates. Figure 4 shows the plot of the temperature vs activation energy for the case of WTO oxidation at a heating rate of 10 °C/min, and the three stages observed in the DTG plot can also be observed here. As the sample is heated from room temperature,  $E$  rises slowly until it reaches a peak value of 410 kJ/mol, which is observed at the peak of the LTO stage after which  $E$  slowly falls to a plateau and then rises in the MTO stage reaching a higher peak value of 581 kJ/mol. The peak  $E$  observed in the HTO stage is lower than those in the LTO and MTO stages at 395 kJ/mol as the rate of mass loss observed from the DTG plots decreases toward the end.

**3.4. FTIR Analysis of Evolved Gases.** The three-dimensional FTIR spectra of the evolved gases in the TGA furnace during pyrolysis and oxidation of WTO at 10 and 20 °C/min are presented in Figure 5. The absorbance value corresponds to the vibrational modes of the various functional groups present in the gases, which are displayed as a function of the time and the wavenumber in different axes. The spectra display a number of peaks within 4000–500  $\text{cm}^{-1}$  from which a qualitative analysis of the composition of the gases at each moment can be identified. Also, the gradual or abrupt changes

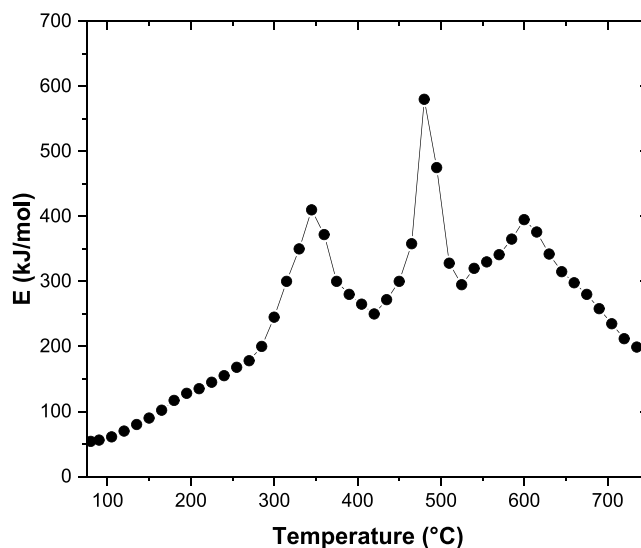


**Figure 4.** Plot of temperature vs activation energy ( $E$ ) for WTO oxidation at 10 °C/min.

in composition of the evolved gases with respect to the furnace temperature can also be estimated. From Figure 5, major differences in the position and the wavenumber of peaks can be noticed between pyrolysis and oxidation, where the evolved gases are completely different from each other. The following sections discuss the evolution of stable pollutant gases released during oxidation and hydrocarbon/oxygenated functional groups evolved during pyrolysis.

**3.4.1. Emission of Pollutant Gases.** The combustion products of WTO were evaluated using FTIR spectroscopy<sup>32</sup> to understand the emission of pollutant gases like  $\text{CO}_2$ ,  $\text{CO}$ ,  $\text{NO}$ , and  $\text{H}_2\text{O}$  for the mentioned heating rates. The FTIR spectra are represented in the form of absorbance, which corresponds to the bonds and functional groups that exist in the evolved gases. The emission data provides a valuable insight to design better combustors and estimate emissions.<sup>33</sup> The assignment of the IR absorbance bands for the discussed pollutant gases is presented in Table 2.

Figure 6a shows the emission data of  $\text{CO}_2$  at various furnace temperatures for the oxidation of WTO. The absorbance unit is presented in the form of absorbance/mg of WTO for all the gases. The  $\text{CO}_2$  emission increases gradually with a noticeable onset near 140 °C at 20 °C/min. This can be compared to the devolatilization and the subsequent oxidation of the alkane/alkene compounds and the paraffinic side chains of aromatic/naphthenic species<sup>27,34</sup> in WTO corresponding to the LTO stage. At 20 °C/min, it reaches its peak at 600 °C, which indicates the beginning of the HTO stage. This stage is more prominent compared to other stages and also dominating due to the burning of char. This is because char consists of mostly elemental carbon and its oxidation leads to more  $\text{CO}_2$  per unit mass.<sup>35</sup> The emission of  $\text{CO}_2$  is reduced drastically with a further increase in temperature because of the depletion of char. Almost all of the WTO components are exhausted at 710 °C. A similar phenomenon is also observed at 5 and 10 °C/min heating rates. The maximum emission of  $\text{CO}_2$  is obtained at 450 and 515 °C for heating rates of 5 and 10 °C/min, respectively. The absorbance value associated with  $\text{CO}_2$  gas is significantly higher compared to the other gases. Some minor fractions of  $\text{CO}_2$  are observed even after 710 °C, which is the indication of remaining  $\text{CO}_2$  in the IR cell.

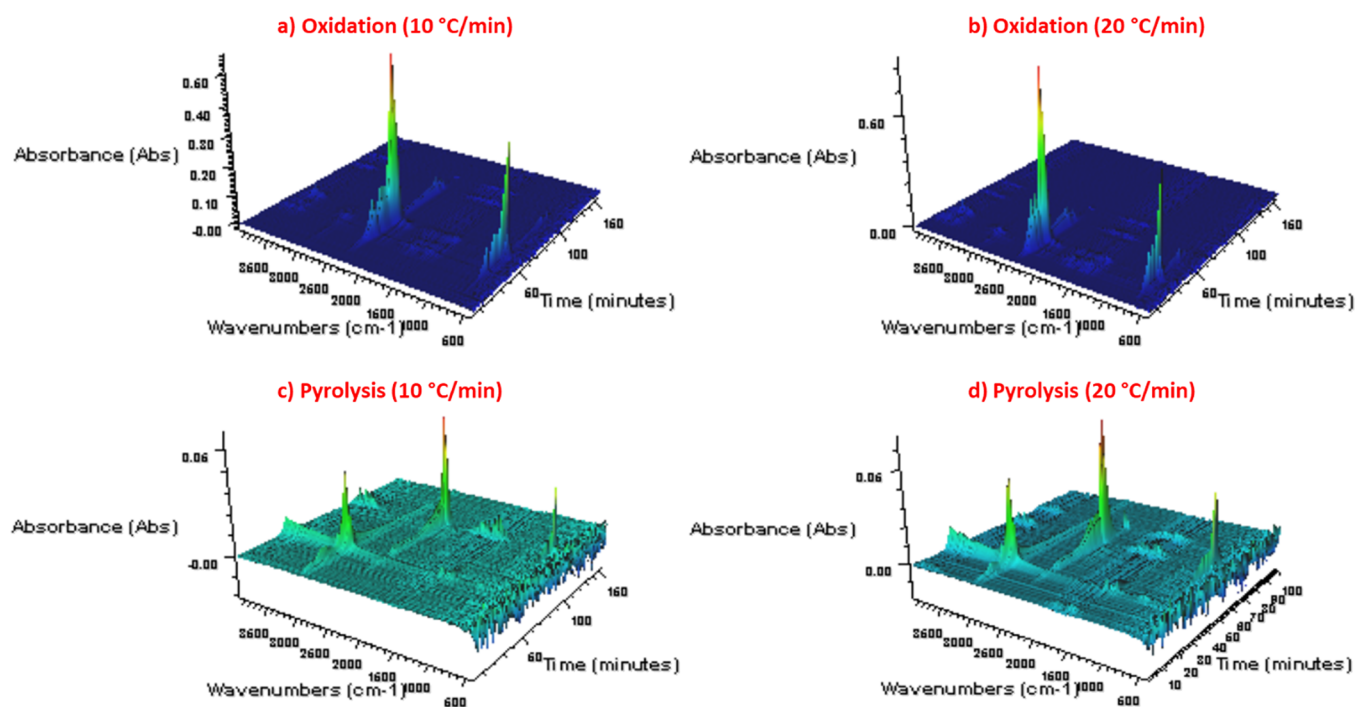


**Figure 5.** Three-dimensional FTIR spectra of the evolved gases in the TGA furnace during (a) oxidation at 10 °C/min, (b) oxidation at 20 °C/min, (c) pyrolysis at 10 °C/min, and (d) pyrolysis at 20 °C/min.

**Table 2.** IR Band Assignment for the Pollutant Gases

wavenumber range (cm <sup>-1</sup> )	selected wavenumber (cm <sup>-1</sup> )	nature	assigned gas
2400–2224	2361	asymmetric stretching of O=C=O bonds	CO <sub>2</sub>
2180–2108	2119	stretching of CO bonds	CO
1762	1762		NO
3500–4000	3556	stretching of O–H bonds	H <sub>2</sub> O

Adapted with permission from ref 15. Copyright 2017 Elsevier.

The emission of CO at various heating rates is shown in Figure 6b. The first formation of CO is observed at 160 °C. The release of CO from WTO has been attributed to the oxidation of organic compounds like stearic acid and extender oils present in the parent tire.<sup>9</sup> This happens during the decarboxylation reaction, which indicates the breakage of carbonyl groups. The first minor peak is observed around 175 °C corresponding to the LTO phase. The peak value of the CO absorbance is observed near 448, 492, and 546 °C at 5, 10, and 20 °C/min, respectively. This is the HTO phase where the burning rate of char is maximum. Then, CO emissions reduce until the temperature reaches 610 °C. The absorbance value of CO is at least 25 times lower than that of CO<sub>2</sub>.

Nitric oxide (NO) and nitrogen dioxide (NO<sub>2</sub>) are both released during combustion, but the vast majority comprises NO.<sup>36</sup> The assigned absorbance peak for NO is 1762 cm<sup>-1</sup>. The emission profile of NO is illustrated in Figure 6c at various temperatures and heating rates. The organically bound nitrogen is released during the devolatilization, which also forms NH<sub>3</sub> or HCN by thermal decomposition.<sup>37</sup> These intermediate species behave like a free radical and react with other free radicals like O<sup>-</sup> and OH<sup>-</sup> and hence form nitrogen oxide (NO). From Figure 6c, it can be inferred that the formation of nitrogen starts at 215 °C, and it increases

gradually. Maximum NO formation is observed near 407, 479, and 524 °C for 5, 10, and 20 °C/min, respectively. This corresponds to the HTO phase. A portion of nitrogen in WTO is not released during devolatilization as it is bounded to char and only evolves during high-temperature oxidation.<sup>35</sup> The release of NO follows a decreasing pattern after reaching the peak.

The emission of H<sub>2</sub>O vapor data is provided in Figure 6d, which was assigned an absorbance peak of 3566 cm<sup>-1</sup>.<sup>19</sup> A flat line is observed in the range of 75–155 °C, which indicates the absence of water vapor in the initial stage. After 155 °C, the water vapor starts to be released representing the middle of the LTO stage. As the temperature rises, the absorbance of water vapor starts to increase and reaches to the maximum point at 421, 465, and 517 °C for heating rates of 5, 10, and 20 °C/min, respectively. Then, it starts to decrease steadily due to the low hydrogen content in char as compared to the volatiles.

**3.4.2. Emission of Functional Groups.** The evolved gases during the pyrolysis of WTO under a nitrogen environment were analyzed in this section in terms of four functional groups, which are alkanes, alkenes, aromatics, and carbonyl groups. Analysis of these functional groups indicates the thermal decomposition reactions occurring during pyrolysis, and this information could help optimize gasifier conditions<sup>38</sup> such that high-value gases could be obtained while minimizing emissions. The functional groups present in a fuel often dictate its properties,<sup>39–43</sup> and the evolved groups dictate the propensity to form soot.<sup>40,44,45</sup> The IR band assignments for the aforementioned functional groups are provided in Table 3 including the selected wavenumber for each functional group.

Alkanes are saturated molecules formed by the hydrogenation of alkenes that are released during pyrolysis as a result of the alpha bond scission. They are also shown to be formed as a result of bond cleavage between the alpha and beta carbon atoms. The IR absorbance peak for alkanes was selected to be

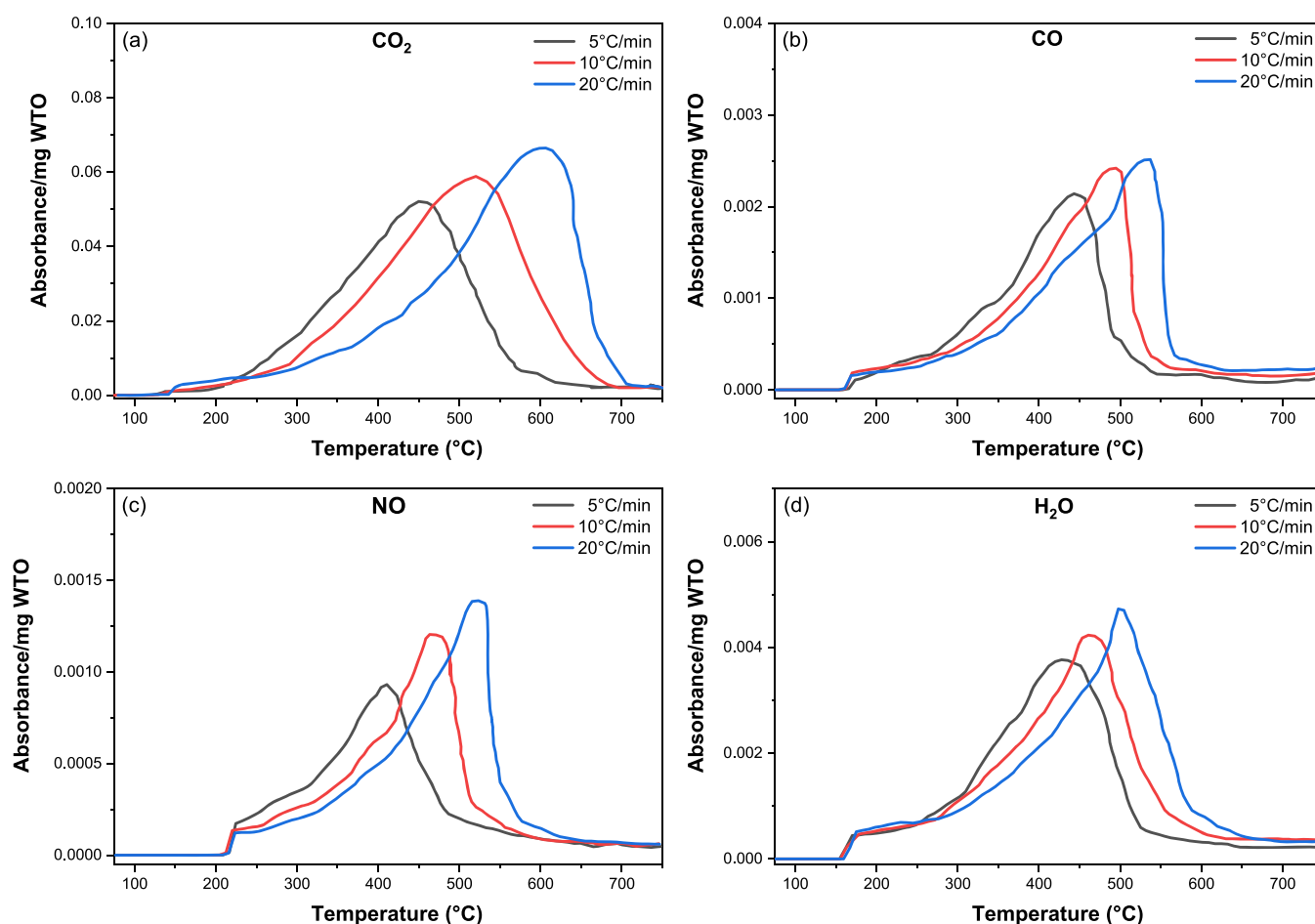


Figure 6. Pollutant gases evolved during the oxidation of the WTO sample. (a)  $\text{CO}_2$ , (b)  $\text{CO}$ , (c)  $\text{NO}$ , and (d)  $\text{H}_2\text{O}$ .

Table 3. IR Band Assignment for the Various Functional Groups

wavenumber range ( $\text{cm}^{-1}$ )	selected wavenumber ( $\text{cm}^{-1}$ )	nature	functional group
2970–2950 2935–2915	2968, 2920	symmetric and asymmetric stretching of methyl and methylene groups	alkanes
3040–3010	3018	C–H stretching of alkene groups C=C stretching of alkene groups	alkenes
3130–3070	3079	C–H bending of aromatics C=C stretching of aromatics	aromatics
1750–1680	1705	carbonyl (C=O) groups	ketones and aldehydes

Adapted with permission from ref 15. Copyright 2017 Elsevier.

$3968\text{ cm}^{-1}$ , and their evolution during WTO pyrolysis in the presence of nitrogen is shown in Figure 7a. The presence of heavy metals like Ni, Fe, and CO in WTO tends to catalyze the pyrolysis and increases the rate of char gasification and syngas formation.<sup>38</sup> The maximum release of the alkane compounds is indicated by the following temperatures of 340, 403, and 459 °C at 5, 10, and 20 °C/min, respectively. Then, the release of alkanes declines gradually. A small amount of alkanes is also detected beyond the second phase of the devolatilization as evidenced by the low absorbance values after 600 °C. This is

mostly due to the presence of the alkanes that may have condensed in the transfer line.

Figure 7b shows the emission profile of alkenes during the pyrolysis of WTO at different heating rates. As shown by Hillier et al.,<sup>47</sup> alkenes are likely formed due to bond scission of alpha carbon and the aromatic ring. The fraction of alkenes detected is very small compared to the alkanes evolved during pyrolysis. Alkenes and cycloalkenes have been observed to be the first group of hydrocarbon species formed during the pyrolysis of tires to produce WTO.<sup>22</sup> The IR absorbance peak selected for alkenes is  $3018\text{ cm}^{-1}$ . They are first noticed at 145 °C because of the breakage of the alkyl chain during devolatilization. It reaches peak values near 340, 368, and 406 °C for 5, 10, and 20 °C/min, respectively. This corresponds to the second phase of the devolatilization noted during pyrolysis. The absorbance values decrease sharply after this point.

The evolution of aromatics during the pyrolysis of WTO is illustrated in Figure 7c. Of all the four groups discussed here, aromatic groups remain the least reactive. As observed from the figure, low fractions of aromatic groups are evolved in the first phase of the devolatilization. This is the reason why many studies<sup>38,48,49</sup> reported in the literature used catalysts like zeolites to promote the conversion of WTO into valuable aromatic hydrocarbons. Aromatic compounds like *para*-xylene and ethylbenzene have been abundantly observed in various WTO samples.<sup>22</sup> As the temperature is further increased, evolution of aromatics increases, which peaks at 312, 340, and

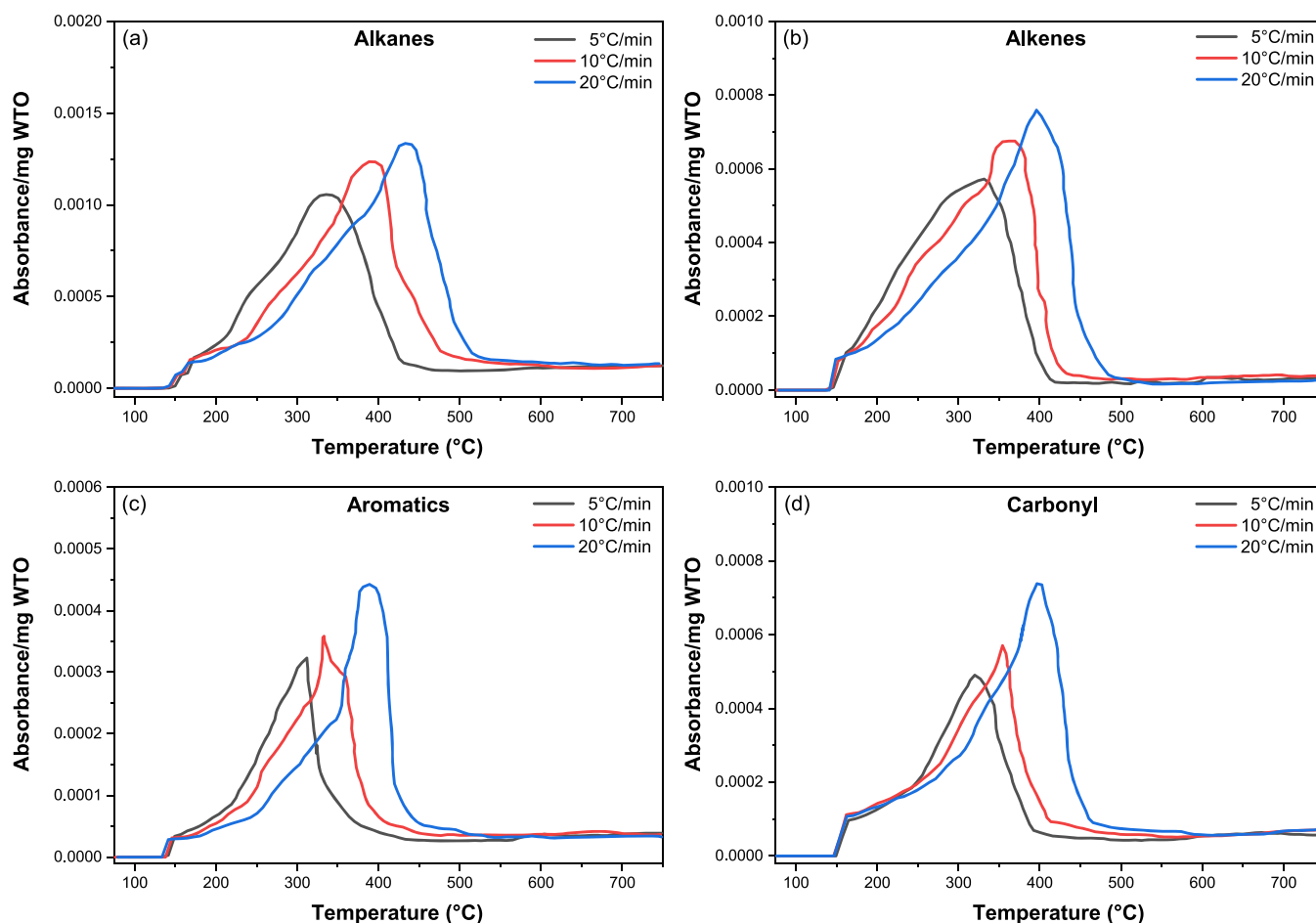


**Figure 7.** Functional groups evolved during the pyrolysis of the WTO sample. (a) Alkanes, (b) alkenes, (c) aromatics, and (d) carbonyl.

385 °C for 5, 10, and 20 °C/min, respectively. Low and continuous absorbance signals are detected after 500 °C. This is most probably due to the aromatics present in the transfer line, and with time, they get re-evaporated as a consequence of the nitrogen carrier gas that constantly flows from the furnace to the FTIR cell.

Ketone functional groups are formed because of the thermal degradation of WTO, they later undergo isomerization reactions to yield aldehydes, and these groups usually remain unseen on the FTIR spectra.<sup>19</sup> Carbonyl groups (C=O) detected at a wavenumber of 1705  $\text{cm}^{-1}$  usually represent both ketones and aldehydes together. The evolution of carbonyl groups in the pyrolysis of WTO at various temperatures is demonstrated in Figure 7d. The maximum evolution is observed near 325, 359, and 412 °C for 5, 10, and 20 °C/min, respectively. The absorbance signals observed for carbonyl groups are lower than that of alkenes but slightly greater than that of the aromatic groups.

#### 4. CONCLUSIONS

Pyrolysis and oxidation of waste tire oil (WTO) have been reported in this current work. Pyrolysis and oxidation of a WTO sample were carried out using a TGA-FTIR system. The analysis was carried out at 5, 10, and 20 °C/min as the three heating rates. During pyrolysis, two devolatilization phases were observed where alkyl chains were depleted in phase one and high-boiling aromatics were released during phase two. A peak mass loss was noted during the second phase, and the

observed values were 4.1, 8.05, and 16.4%/min at temperatures of 322, 340, and 359 °C, respectively. Subsequently, for oxidation, three stages, namely, LTO, MTO, and HTO, were observed by means of TG/DTG curves. The maximum weight loss was obtained during the HTO phase where char oxidation occurred. Peak mass loss values of 1.45, 1.91, and 2.89%/min were noticed at 5, 10, and 20 °C/min during the HTO phase, at the end of which an ash-like sample weighing 0.4–0.5% of the initial weight was left behind. Kinetic analysis was performed to estimate the activation energies ( $E$ ) at various stages. During WTO oxidation at 10 °C/min, a peak  $E$  value of 581 kJ/mol was obtained during the MTO stage. The emission of the pollutant gases ( $\text{CO}_2$ , CO, NO, and  $\text{H}_2\text{O}$ ) was analyzed by means of absorbance/mg of sample.  $\text{CO}_2$  had the highest emission during the oxidation as expected, and its absorbance value was almost 25 times higher than that of CO. Finally, the evolution of functional group (alkanes, alkenes, aromatics, and carbonyl groups) was examined during the pyrolysis of WTO. Alkanes were the most prevalent groups whereas aromatics were the least detected groups in the analyzed gases. The obtained information can help in the better design of gasifiers and combustors to maximize the formation of high-value products and minimize emissions.

#### ■ AUTHOR INFORMATION

##### Corresponding Authors

Abdul Gani Abdul Jameel – Department of Chemical Engineering and Center for Refining & Advanced Chemicals,

King Fahd University of Petroleum and Minerals, Dhahran 31261, Saudi Arabia; [orcid.org/0000-0003-2219-4814](https://orcid.org/0000-0003-2219-4814); Email: [a.abduljameel@kfupm.edu.sa](mailto:a.abduljameel@kfupm.edu.sa)

**Usama Ahmed** – Department of Chemical Engineering and Interdisciplinary Research Center for Hydrogen and Energy Storage, King Fahd University of Petroleum and Minerals, Dhahran 31261, Saudi Arabia; [orcid.org/0000-0001-7199-600X](https://orcid.org/0000-0001-7199-600X); Email: [usama.ahmed@kfupm.edu.sa](mailto:usama.ahmed@kfupm.edu.sa)

## Authors

**Awad B.S. Alqaity** – Department of Mechanical Engineering and Interdisciplinary Research Center for Hydrogen and Energy Storage, King Fahd University of Petroleum and Minerals, Dhahran 31261, Saudi Arabia

**KM Oajedul Islam** – Department of Chemical Engineering, King Fahd University of Petroleum and Minerals, Dhahran 31261, Saudi Arabia

**Amjad Ali Pasha** – Aerospace Engineering Department, King Abdulaziz University, Jeddah 21589, Saudi Arabia

**Sikandar Khan** – Department of Mechanical Engineering, King Fahd University of Petroleum and Minerals, Dhahran 31261, Saudi Arabia

**Medhat A. Nemitallah** – Department of Mechanical Engineering and Interdisciplinary Research Center for Hydrogen and Energy Storage, King Fahd University of Petroleum and Minerals, Dhahran 31261, Saudi Arabia; K.A. CARE Energy Research & Innovation Center, Dhahran 31261, Saudi Arabia; [orcid.org/0000-0001-9075-2844](https://orcid.org/0000-0001-9075-2844)

Complete contact information is available at:

<https://pubs.acs.org/10.1021/acsomega.2c01366>

## Notes

The authors declare no competing financial interest.

## ACKNOWLEDGMENTS

The authors would like to acknowledge support provided by the Deanship of Research Oversight and Coordination (DROC) at the King Fahd University of Petroleum & Minerals (KFUPM) for funding this work through project no. DF201017.

## REFERENCES

- (1) Osorio-Vargas, P.; Lick, I. D.; Sobrevía, F.; Correa-Muriel, D.; Menares, T.; Manrique, R.; Casella, M. L.; Arteaga-Pérez, L. E. Thermal Behavior, Reaction Pathways and Kinetic Implications of Using a Ni/SiO<sub>2</sub> Catalyst for Waste Tire Pyrolysis. *Waste Biomass Valoriz.* **2021**, *12*, 6465–6479.
- (2) Larionov, K. B.; Slyusarskiy, K. V.; Tsublinskiy, S. A.; Kaltaev, A. Z.; Berezikov, N. I.; Gorshkov, A. S.; Lavrinenko, S. V.; Gubin, V. E. Activation of Anthracite Combustion Using Pyrolysis Oil from Thermal Conversion of Waste Car Tires. *ACS Omega* **2021**, *6*, 19731–19739.
- (3) Campuzano, F.; Abdul Jameel, A. G.; Zhang, W.; Emwas, A.-H.; Agudelo, A. F.; Martínez, J. D.; Sarathy, S. M. Fuel and Chemical Properties of Waste Tire Pyrolysis Oil Derived from a Continuous Twin-Auger Reactor. *Energy Fuels* **2020**, *34*, 12688–12702.
- (4) Campuzano, F.; Abdul Jameel, A. G.; Zhang, W.; Emwas, A.; Agudelo, A. F.; Martínez, J. D.; Sarathy, S. M. On the Distillation of Waste Tire Pyrolysis Oil: A Structural Characterization of the Derived Fractions. *Fuel* **2021**, *290*, No. 120041.
- (5) Karagöz, M.; Ağbulut, Ü.; Sarıdemir, S. Waste to Energy: Production of Waste Tire Pyrolysis Oil and Comprehensive Analysis of Its Usability in Diesel Engines. *Fuel* **2020**, *275*, No. 117844.
- (6) Kebritchi, A.; Firoozifar, H.; Shams, K.; Jalali-Arani, A. Effect of Pre-Devulcanization and Temperature on Physical and Chemical

Properties of Waste Tire Pyrolytic Oil Residue. *Fuel* **2013**, *112*, 319–325.

(7) Díez, C.; Martínez, O.; Calvo, L. F.; Cara, J.; Morán, A. Pyrolysis of Tyres. Influence of the Final Temperature of the Process on Emissions and the Calorific Value of the Products Recovered. *Waste Manage.* **2004**, *24*, 463–469.

(8) Aguado, R.; Olazar, M.; Vélez, D.; Arabiourrutia, M.; Bilbao, J. Kinetics of Scrap Tyre Pyrolysis under Fast Heating Conditions. *J. Anal. Appl. Pyrolysis* **2005**, *73*, 290–298.

(9) Čepić, Z.; Mihajlović, V.; Đurić, S.; Milotić, M.; Stošić, M.; Stepanov, B.; Ilić Mićunović, M. Experimental Analysis of Temperature Influence on Waste Tire Pyrolysis. *Energies* **2021**, *14*, 5403.

(10) Pan, D.; Jiang, W.; Guo, R.; Huang, Y.; Pan, W. Thermogravimetric and Kinetic Analysis of Co-Combustion of Waste Tires and Coal Blends. *ACS Omega* **2021**, *6*, 5479–5484.

(11) Lin, Y.; Liao, Y.; Yu, Z.; Fang, S.; Lin, Y.; Fan, Y.; Peng, X.; Ma, X. Co-Pyrolysis Kinetics of Sewage Sludge and Oil Shale Thermal Decomposition Using TGA–FTIR Analysis. *Energy Convers. Manage.* **2016**, *118*, 345–352.

(12) Kanca, A. Investigation on Pyrolysis and Combustion Characteristics of Low Quality Lignite, Cotton Waste, and Their Blends by TGA-FTIR. *Fuel* **2020**, *263*, No. 116517.

(13) Li, H.; Niu, S.; Lu, C.; Wang, Y. Comprehensive Investigation of the Thermal Degradation Characteristics of Biodiesel and Its Feedstock Oil through TGA–FTIR. *Energy Fuels* **2015**, *29*, 5145–5153.

(14) Ma, Z.; Wang, J.; Yang, Y.; Zhang, Y.; Zhao, C.; Yu, Y.; Wang, S. Comparison of the Thermal Degradation Behaviors and Kinetics of Palm Oil Waste under Nitrogen and Air Atmosphere in TGA-FTIR with a Complementary Use of Model-Free and Model-Fitting Approaches. *J. Anal. Appl. Pyrolysis* **2018**, *134*, 12–24.

(15) Abdul Jameel, A. G.; Han, Y.; Brignoli, O.; Telalović, S.; Elbaz, A. M.; Im, H. G.; Roberts, W. L.; Sarathy, S. M. Heavy Fuel Oil Pyrolysis and Combustion: Kinetics and Evolved Gases Investigated by TGA-FTIR. *J. Anal. Appl. Pyrolysis* **2017**, *127*, 183–195.

(16) Wang, D.; Xiao, R.; Zhang, H.; He, G. Comparison of Catalytic Pyrolysis of Biomass with MCM-41 and CaO Catalysts by Using TGA-FTIR Analysis. *J. Anal. Appl. Pyrolysis* **2010**, *89*, 171–177.

(17) Parshetti, G. K.; Quek, A.; Betha, R.; Balasubramanian, R. TGA–FTIR Investigation of Co-Combustion Characteristics of Blends of Hydrothermally Carbonized Oil Palm Biomass (EFB) and Coal. *Fuel Process. Technol.* **2014**, *118*, 228–234.

(18) Ordonez-Loza, J.; Chejne, F.; Jameel, A. G. A.; Telalovic, S.; Arrieta, A. A.; Sarathy, S. M. An Investigation into the Pyrolysis and Oxidation of Bio-Oil from Sugarcane Bagasse: Kinetics and Evolved Gases Using TGA-FTIR. *J. Environ. Chem. Eng.* **2021**, *9*, No. 106144.

(19) Gómez-Siurana, A.; Marcilla, A.; Beltrán, M.; Berenguer, D.; Martínez-Castellanos, I.; Menargues, S. TGA/FTIR Study of Tobacco and Glycerol–Tobacco Mixtures. *Thermochim. Acta* **2013**, *573*, 146–157.

(20) Xu, F.; Wang, B.; Yang, D.; Ming, X.; Jiang, Y.; Hao, J.; Qiao, Y.; Tian, Y. TG-FTIR and Py-GC/MS Study on Pyrolysis Mechanism and Products Distribution of Waste Bicycle Tire. *Energy Convers. Manage.* **2018**, *175*, 288–297.

(21) Menares, T.; Herrera, J.; Romero, R.; Osorio, P.; Arteaga-Pérez, L. E. Waste Tires Pyrolysis Kinetics and Reaction Mechanisms Explained by TGA and Py-GC/MS under Kinetically-Controlled Regime. *Waste Manage.* **2020**, *102*, 21–29.

(22) Li, D.; Lei, S.; Lin, F.; Zhong, L.; Ma, W.; Chen, G. Study of Scrap Tires Pyrolysis – Products Distribution and Mechanism. *Energy* **2020**, *213*, No. 119038.

(23) Czajczyńska, D.; Czajka, K.; Krzyżyńska, R.; Jouhara, H. Waste Tyre Pyrolysis – Impact of the Process and Its Products on the Environment. *Therm. Sci. Eng. Prog.* **2020**, *20*, No. 100690.

(24) Elbaz, A. M.; Gani, A.; Hourani, N.; Emwas, A.-H.; Sarathy, S. M.; Roberts, W. L. TG/DTG, FT-ICR Mass Spectrometry, and NMR Spectroscopy Study of Heavy Fuel Oil. *Energy Fuels* **2015**, *29*, 7825–7835.

- (25) Khateeb, A. A.; Elbaz, A. M.; Guida, P.; Roberts, W. L. Influence of Asphaltene Concentration on the Combustion of a Heavy Fuel Oil Droplet. *Energy Fuels* **2018**, *32*, 12981–12991.
- (26) Saravanan, V.; Aravind, A.; Jayanti, S. Burning Profile of High Ash Indian Coals in Oxy-Fuel Environment. *ASME Int. Mech. Eng. Congr. Expo.* **2008**, 48647, 119–131.
- (27) Crnkovic, P. M.; Leiva, C. R. M.; dos Santos, A. M.; Milioli, F. E. Kinetic Study of the Oxidative Degradation of Brazilian Fuel Oils. *Energy Fuels* **2007**, *21*, 3415–3419.
- (28) Han, Y.; Elbaz, A. M.; Roberts, W. L.; Im, H. G. New Procedure to Develop Lumped Kinetic Models for Heavy Fuel Oil Combustion. *Energy Fuels* **2016**, *30*, 9814–9818.
- (29) Fan, C.; Zan, C.; Zhang, Q.; Ma, D.; Chu, Y.; Jiang, H.; Shi, L.; Wei, F. The Oxidation of Heavy Oil: Thermogravimetric Analysis and Non-Isothermal Kinetics Using the Distributed Activation Energy Model. *Fuel Process. Technol.* **2014**, *119*, 146–150.
- (30) Miura, K. A New and Simple Method to Estimate  $f(E)$  and  $K_0(E)$  in the Distributed Activation Energy Model from Three Sets of Experimental Data. *Energy Fuels* **1995**, *9*, 302–307.
- (31) Miura, K.; Maki, T. A Simple Method for Estimating  $f(E)$  and  $k_0(E)$  in the Distributed Activation Energy Model. *Energy Fuels* **1998**, *12*, 864–869.
- (32) Palani, R.; AbdulGani, A.; Balasubramanian, N. Treatment of Tannery Effluent Using a Rotating Disc Electrochemical Reactor. *Water Environ. Res.* **2017**, *89*, 77–85.
- (33) Khalafalla, S. S.; Zahid, U.; Abdul Jameel, A. G.; Ahmed, U.; Alenazey, F. S.; Lee, C. Conceptual Design Development of Coal-to-Methanol Process with Carbon Capture and Utilization. *Energies* **2020**, *13*, 6421.
- (34) Zhang, H. R.; Eddings, E. G.; Sarofim, A. F. Pollutant Emissions from Gasoline Combustion. 1. Dependence on Fuel Structural Functionalities. *Environ. Sci. Technol.* **2008**, *42*, 5615–5621.
- (35) Selcuk, N.; Yuzbasi, N. S. Combustion Behaviour of Turkish Lignite in O<sub>2</sub>/N<sub>2</sub> and O<sub>2</sub>/CO<sub>2</sub> Mixtures by Using TGA–FTIR. *J. Anal. Appl. Pyrolysis* **2011**, *90*, 133–139.
- (36) Wu, S.-R.; Chang, W.-C.; Chiao, J. Low NO<sub>x</sub> Heavy Fuel Oil Combustion with High Temperature Air. *Fuel* **2007**, *86*, 820–828.
- (37) Lehtoranta, K.; Vesala, H.; Koponen, P.; Korhonen, S. Selective Catalytic Reduction Operation with Heavy Fuel Oil: NO<sub>x</sub>, NH<sub>3</sub>, and Particle Emissions. *Environ. Sci. Technol.* **2015**, *49*, 4735–4741.
- (38) Portofino, S.; Casu, S.; Iovane, P.; Russo, A.; Martino, M.; Donatelli, A.; Galvagno, S. Optimizing H<sub>2</sub> Production from Waste Tires via Combined Steam Gasification and Catalytic Reforming. *Energy Fuels* **2011**, *25*, 2232–2241.
- (39) Aljaman, B.; Ahmed, U.; Zahid, U.; Reddy, V. M.; Sarathy, S. M.; Abdul Jameel, A. G. A Comprehensive Neural Network Model for Predicting Flash Point of Oxygenated Fuels Using a Functional Group Approach. *Fuel* **2022**, *317*, No. 123428.
- (40) Abdul Jameel, A. G. A. Predicting Sooting Propensity of Oxygenated Fuels Using Artificial Neural Networks. *Processes* **2021**, *9*, 1070.
- (41) Abdul Jameel, A. G. A Functional Group Approach for Predicting Fuel Properties, King Abdullah University of Science and Technology, 2019. DOI: 10.25781/KAUST-ZBB21.
- (42) Ilies, B. D.; Khandavilli, M.; Li, Y.; Kukkadapu, G.; Wagnon, S. W.; Abdul Jameel, A. G.; Sarathy, S. M. Probing the Chemical Kinetics of Minimalist Functional Group Gasoline Surrogates. *Energy Fuels* **2021**, *35*, 3315–3332.
- (43) Abdul Jameel, A. G. Identification and Quantification of Hydrocarbon Functional Groups in Gasoline Using 1H-NMR Spectroscopy for Property Prediction. *Molecules* **2021**, *26*, 6989.
- (44) Pei, X.; Abdul Jameel, A. G.; Chen, C.; AlGhamdi, I. A.; AlAhmadi, K.; AlBarakati, E.; Saxena, S.; Roberts, W. L. Swirling Flame Combustion of Heavy Fuel Oil: Effect of Fuel Sulfur Content. *J. Energy Resour. Technol.* **2021**, *143*, 1–16.
- (45) Abdul Jameel, A. G.; Alkhateeb, A.; Telalović, S.; Elbaz, A. M.; Roberts, W. L.; Sarathy, S. M. Environmental Challenges and Opportunities in Marine Engine Heavy Fuel Oil Combustion. In *Proceedings of the Fourth International Conference in Ocean Engineering*; Springer, 2019; pp. 1047–1055. DOI: 10.1007/978-981-13-3119-0\_72.
- (46) Ma, Z.; Chen, D.; Gu, J.; Bao, B.; Zhang, Q. Determination of Pyrolysis Characteristics and Kinetics of Palm Kernel Shell Using TGA – FTIR and Model-Free Integral Methods. *Energy Convers. Manage.* **2015**, *89*, 251–259.
- (47) Hillier, J. L.; Fletcher, T. H.; Solum, M. S.; Pugmire, R. J. Characterization of Macromolecular Structure of Pyrolysis Products from a Colorado Green River Oil Shale. *Ind. Eng. Chem. Res.* **2013**, *52*, 15522–15532.
- (48) Williams, P. T.; Brindle, A. J. Aromatic Chemicals from the Catalytic Pyrolysis of Scrap Tyres. *J. Anal. Appl. Pyrolysis* **2003**, *67*, 143–164.
- (49) Shen, B.; Wu, C.; Wang, R.; Guo, B.; Liang, C. Pyrolysis of Scrap Tyres with Zeolite USY. *J. Hazard. Mater.* **2006**, *137*, 1065–1073.